

C-point Singularities in Poincaré Beams

Enrique J. Galvez, Brett L. Rojec, Kory Beach, and Xinru Cheng

Department of Physics and Astronomy, Colgate University, Hamilton, NY 13346, USA.
egalvez@colgate.edu

Abstract: We present the study of new optical modes of Poincaré beams that have polarization-singularity C-points in their axis. We do so by preparing tailored optical beams in non-separable linear superpositions of spatial and polarization modes. We present the production of an asymmetric type of polarization-singularity C-points, known as monstars. This type of C-point can be produced by the superposition of two beams, one with an asymmetric optical vortex, and a second one in a fundamental Gaussian mode, both in orthogonal circular polarization states.

OCIS codes: (260.5430) Polarization; (260.6042) Singular Optics

1. Introduction

Polarization singularities are a type of optical singularities that arise when one of the parameters specifying the polarization of the light is undefined [1]. In particular, C-points are singularities present in a field of polarization ellipses, where the orientation of the ellipse is undefined. The C-point is in a state of circular polarization. Surrounding it is a field of ellipses whose semi-major axis rotates about the C-point. This divides the C-points into two classes: those that rotate with the angular coordinate about the C-point, and those that rotate counter to it. An index representing this rotation about the C-point is I_C . Since ellipses' axes are not directional (i.e., are the ellipse is the same for a reflection about one of its axes), the minimum rotation is half a turn, and so the smallest absolute value of I_C is $1/2$. In addition to the rotation, the ellipses form a pattern that can be divided into three classes: lemon, star and monstar. Lemon and monstar have $I_C = +1/2$, and star has $I_C = -1/2$. The distinction between the lemon and the monstar is subtle: the orientation of the semi-major axis matches the angular coordinate (i.e., it is radial) at one (for lemons) or three (for monstars) angular directions. For stars the orientation is radial in three directions.

Figure 1 shows examples of the three distinct patterns of C-points: lemon (a), star (b) and monstar (c). The lines shown are formed by following the directions of the semi-major axis of the ellipses. They are also known as “lines of curvature” due to the analogy with Gaussian surfaces [2], explained below. These types of patterns give rise to the line, or “L,” classification of C-points. These lines of curvature help understand the value of I_C for each case. For cases (a) and (c), a vector aligned with the lines rotates in a counter-clockwise sense for a counter-clockwise circulation around the C-point (see Fig. 1). Conversely, in case (b) a vector rotates in the opposite, clockwise sense, for a counter-clockwise circulation. If the rate of rotation of the semi-major axis is constant along a circular path centered about the C-point, it is easy to see that lemons (Fig. 1a) have only one direction where the semi-major axis is radial: the semi-major axis rotates at half the rate of circulation about the C-point, and so there is undoubtedly one direction where the axis has to point to the center. The same is true with the star (Fig. 1b): since it rotates in the sense opposite to the path, the axis must be radial in three places. For the monstar (Fig. 1c) the pattern is not obvious. This is because the monstar is part of a more general class of C-points where the rate of rotation of the semi-major axis is not constant: the rotation rate may be greater and lower than the circulation rate, creating more than one angular directions where the polarization ellipses' axes are radial. In Fig. 1c there are three angles where this is true. These radial directions are separatrices of line morphologies. Note also something unique about the monstar in Fig. 1c: in two of the sectors delineated by the separatrices, all the lines of curvature have the C-point as an end point.

There is an interesting parallel between a field of polarization singularities of light and the topology of surfaces with umbilic points [2]. In this case, the ellipticity of the polarization ellipses and their orientation is correlated with the principal curvatures of a surface. When the surface curvature is approximated by cubic corrections to a quadratic form, the umbilic points, of degenerate (purely spherical) curvature, correspond to the C-points. In this situation, the distinct classes of umbilics are found in the solutions to the cubic equation [2]. We approach the problem in a similar way, creating a situation that defines a pattern of ellipses around a C-point, and find a cubic equation that classifies the distinct types of C-points [3].

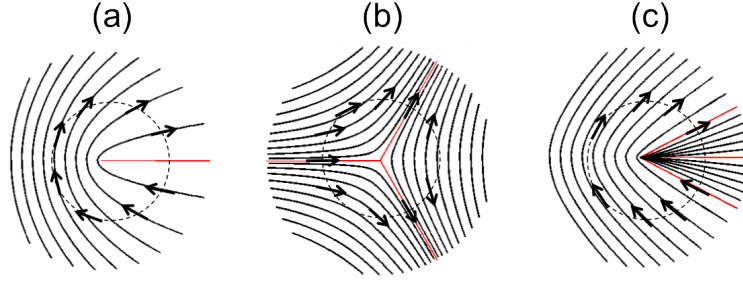


Fig. 1. The three types of C-points: lemon (a), star (b) and monstar (c). The solid lines connect the directions of the semi-major axes of the ellipses. The vectors drawn illustrate how they rotate in a circular (dashed-line) path around the C-point.

All three types of polarization singularity C-points have been observed in complex light patterns formed when polarized light traverses inhomogeneous and birefringent media [5–8]. There is also interest in preparing these features deliberately in tailored beams. Lemons and stars have been prepared in tailored beams in three distinct types of situations: passage through an optical element under symmetric stress birefringence [9], passage through an electro-optical element, the “Q-plate” [10]; and by superposition of optical beams in distinct spatial modes with opposite polarization (our approach) [11–13].

We have already produced symmetric polarization singularities deliberately using a polarization interferometer and passive optical elements as part of a general study of the modes of Poincare beams [11]. However, until recently the deliberate production of asymmetric singularities, including monstars, has been elusive. Motivated by a theoretical study [14, 15], we have determined and implemented a method to produce them in the laboratory [3, 4]. This approach relies on the simplest prescription that makes up a C-point: the superposition of an optical vortex in a circularly polarized eigenstate with a plane wave in the orthogonal circularly polarized eigenstate. Thus, production of an asymmetric C-point requires an asymmetric optical vortex. One class of asymmetric optical vortices involves the superposition of two optical vortices of opposite topological charge, which is the method described here. As shown below, we do so using a superposition of Laguerre-Gauss modes of opposite topological charge. Alternatively, superpositions of Hermite-Gauss modes have also been used for the same purpose [4, 13].

2. Theory

In a recent report we determined a method for producing a large range of C-points [3]. We now revise this method to include a wider range of possibilities. At the heart of the argument is the representation of a state of polarization in the circular basis [11]:

$$\hat{e} = e^{i\theta} \cos \chi \hat{e}_R + e^{-i\theta} \sin \chi \hat{e}_L, \quad (1)$$

where \hat{e}_R and \hat{e}_L represent the states of right and left circular polarization, respectively. The state of Eq. 1 has an ellipticity given by $\varepsilon = b/a = \tan(\pi/4 - \chi)$, with b and a being the semi-minor and semi-major axes of the ellipse, respectively. The orientation of the semi-major axis is θ . Thus, very conveniently, the ellipticity and orientation of the polarization ellipse are independently determined by the variables χ and θ . These two are, respectively, half the polar and azimuth angles on the Poincaré sphere [11].

As mentioned earlier, a general form of a C-point can be constructed by the superposition of an optical vortex and a plane wave, or

$$\hat{\psi} = f \hat{e}_R + \hat{e}_L, \quad (2)$$

where f represents an optical vortex. For the case of a symmetric C-point, $f = r \exp(i\ell\phi)$ is an optical vortex with topological charge ℓ , and with r and ϕ being the transverse polar coordinates. Symmetric lemons or stars are obtained when ℓ is $+1$ and -1 , respectively. An asymmetric optical vortex can be obtained by combining two optical vortices of opposite topological charge:

$$f = e^{i\phi} \cos \beta + e^{-i\phi} e^{i\gamma} \sin \beta, \quad (3)$$

where $0 \leq \beta \leq \pi/2$ and $0 \leq \gamma \leq 2\pi$ are parameters that control the relative amplitude and phase, respectively. When $0 \leq \beta < \pi/4$ ($\pi/4 < \beta \leq \pi/2$) the vortex is one with $\ell = +1$ ($\ell = -1$), and with a phase gradient that has two

orthogonal symmetry axes, where the rate of change of the phase has a maximum $(1 + \tan \beta)/(1 - \tan \beta)$ when $\phi = \gamma/2$, $\gamma/2 + \pi$, and a minimum $(1 - \tan \beta)/(1 + \tan \beta)$ when $\phi = \gamma/2 + \pi/2$, $\gamma/2 + 3\pi/2$. Figure 2a shows the phase pattern of f , encoded in gray scale, when $\beta = \pi/6$ and $\gamma = \pi$. Note that the phase varies more rapidly near the horizontal axis than near the vertical axis. Function f in Eq 3 can be implemented experimentally via the superposition of two Laguerre-Gauss modes, as shown below.

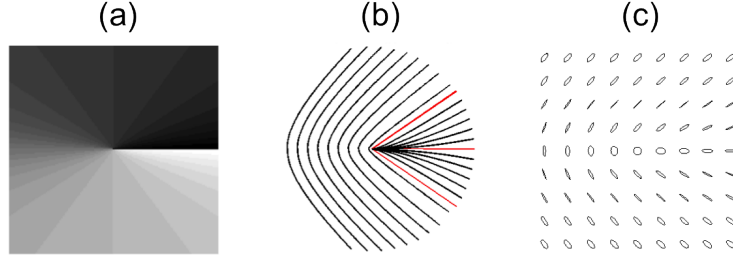


Fig. 2. The making of a monstar C-point with $\beta = \pi/6$ and $\gamma = \pi$. Shown is the phase of the corresponding optical vortex (a): and the line of curvature map (b) and ellipse field (c) of the resulting monstar.

The mechanism to make an asymmetric vortex sets the stage for determining the parameter values that give rise to the range of C-points. According to the arguments above, then, a C-point can be constructed by combining Eqs. 2 and 3:

$$\hat{\psi} = \left(e^{i\phi} \cos \beta + e^{-i\phi} e^{i\gamma} \sin \beta \right) e^{i\delta} \hat{e}_R + \hat{e}_L, \quad (4)$$

where we have added an additional phase δ between the two polarization eigenstates. If we consider the index classification of the C-points, then $\beta = \pi/4$ divides the two evenly: $\beta < \pi/4$ for $I_C = +1/2$ and $\beta > \pi/4$ for $I_C = -1/2$.

As mentioned above, the line classification [2] divides the C-points in terms of the pattern of lines that are tangent to the semi-major axes of the ellipses. Figure 2b shows the line pattern for the case $\beta = \pi/6$ and $\gamma = \pi$ (that of Fig. 1c corresponds to $\beta = 25^\circ$). This pattern corresponds to a C-point monstar. Following Eq. 1, the orientation of the ellipses is half of the relative phase between the two polarization eigenstates in Eq. 4:

$$\phi = \frac{1}{2} \arg \left(f e^{i\delta} \right). \quad (5)$$

This equation is can be rewritten as

$$a_3 x^3 + a_2 x^2 + a_1 x + a_0 = 0, \quad (6)$$

where $x = \tan \phi$, and

$$a_3 = \tan \delta \tan \beta \sin \gamma - \tan \beta \cos \gamma + 1 \quad (7)$$

$$a_2 = 3 \tan \delta \tan \beta \cos \gamma + 3 \tan \beta \sin \gamma - \tan \delta \quad (8)$$

$$a_1 = -3 \tan \delta \tan \beta \sin \gamma + 3 \tan \beta \cos \gamma + 1 \quad (9)$$

$$a_0 = -\tan \delta \tan \beta \cos \gamma - \tan \beta \sin \gamma - \tan \delta \quad (10)$$

Equation 6 can be solved exactly for certain values of β , γ and δ . For example, when $\gamma = 0$ and $\delta = 0$ there is 1 real root for $\beta < \pi/4$ (lemon) and 3 roots for $\beta > \pi/4$ (star). There are no C-points with 3 real roots and a positive index (i.e., a monstar) for this case. For $\gamma = \pi$ and $\delta = 0$ there is 1 real root with positive index for $0 \leq \beta < \tan^{-1}(1/3)$ (lemon), 3 real roots with positive index for $\tan^{-1}(1/3) < \beta < \pi/4$ (monstar), and 3 real roots with negative index for $\pi/4 < \beta \leq \pi/2$ (star). The case $\beta = \tan^{-1}(1/3)$ gives three real degenerate roots, with $\phi = 0$.

Most other cases need to be solved numerically. If we fix $\delta = 0$ we come up with the space of C-points shown by the sphere of Fig. 3. A sphere makes sense because the space is produced by the variables β , the polar angle, and γ , the azimuth angle. In fact, the spatial mode given by f in Fig. 3 can be mapped onto a sphere representing all first-order spatial modes [16]. In our case, we generate all the spatial modes given by f using the polar antipodes, but in general, they can be generated by any two antipodes of the sphere. In a similar fashion, the C-points represented by the sphere of Fig. 3 can be generated by a superposition of any pair of antipodes of that sphere.

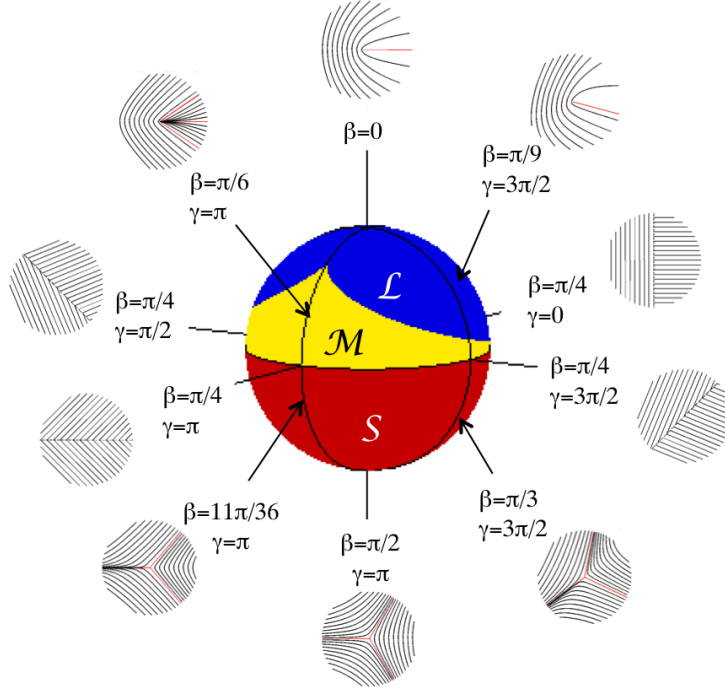


Fig. 3. All C-points generated by Eq. 4 can be mapped on the surface of a sphere, where β is the polar angle and γ is the azimuth angle. The sphere is divided into three regions depending on the type of C-points: lemon (L), monstar (M) and star (S). Patterns corresponding to individual points are shown in the inserts.

The set of points that mark the boundary between lemon and monstar, shown in Fig 3, correspond to cases where the cubic equation of Eq. 6 has three roots, but with more than one being degenerate. Table 1 gives a few values of β of the boundary for assorted values of γ , and fixed $\delta = 0$.

Table 1. C-point parameters for the lemon-monstar boundary. Angles are in degrees.

γ	δ	β
30	0	44.5
60	0	43.0
90	0	40.3
120	0	36.2
150	0	30.0
180	0	18.4
270	45	18.4
180	15	30

The space of C-points shown in Fig. 3 contains all the C-Points that can be produced by isolated vortices. Inserts show the line of curvature maps of assorted examples. The space does not really change when we vary δ . We found that for a non-zero value of δ , the lemon-monstar boundary shifts on the sphere by 2δ (i.e., a 2δ rotation about the polar axis), and the patterns of each point rotate in place by δ . That is, if a C-point on the sphere is defined by (β, γ, δ) , then that C-point is the same as the one in $(\beta, \gamma - 2\delta, 0)$ but rotated by δ (positive is counter-clockwise). Thus, varying δ does not introduce any new morphology. The fractional areas of the three regions remains the same, regardless of δ , at 0.382 for lemon, 0.118 for monstar and 0.5 for star. The space represented by the sphere covers all C-point patterns where the ellipse orientations are purely radial. This is because the only way to place an isolated vortex with topological charge of 1 in the center of the field is via a superposition of concentric $+1$ and -1 vortices, as presented

above. Superpositions with any other topological charges and non-concentricity produces an array of vortices [17, 18], and consequently the phase lines curve from one vortex to the other one(s). The latter effect produces an array of C-points with richer morphology. However, the morphology of a given C-point depends on the neighboring C-points.

3. Apparatus

We performed the experiments with an apparatus designed to produce any C-point described in the previous section. We have analyzed a variety of cases for many values of β . Although we explored a variety of values of γ and δ , our systematic studies focused mostly on $\gamma = \pi$ and $\delta = 0$. The vortices were generated via linear superpositions of concentric Laguerre-Gauss modes.

We used the apparatus of Fig. 4a. Briefly, a vertically polarized laser beam from a helium-neon laser was expanded and spatially filtered to produce a pure Gaussian mode. The resulting beam was split evenly by a non-polarizing beam splitter, which constituted the entrance port of a Mach-Zehnder-type interferometer. Each of these beams eventually encoded the two terms of Eq. 4. One of the beams traveled through a Pancharatnam-Berry phase shifter (see for example Ref. [19]) to precisely change the relative phase δ between the two beams.

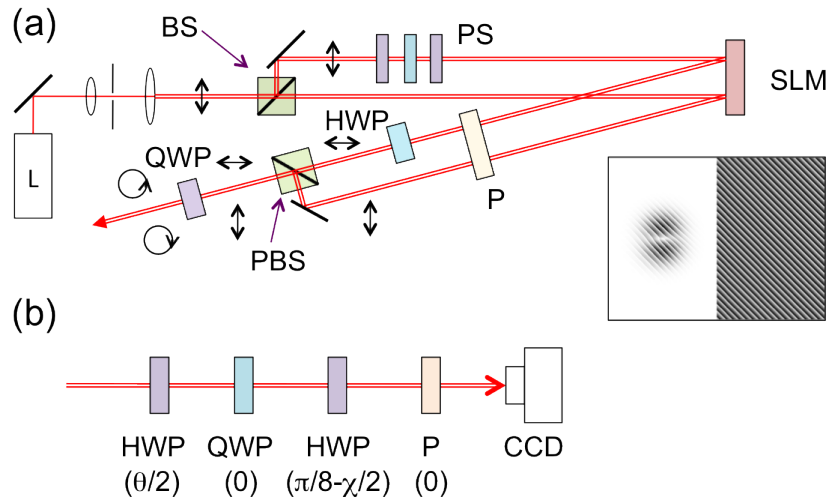


Fig. 4. (a) Apparatus used to make the Poincaré beams bearing a C-point in their axes. Optical components include a non-polarizing beam splitter (BS), polarizing beam splitter (PBS), phase shifter (PS), polarizer (P), half-wave plate (HWP), quarter-wave plate (QWP), laser (L) and spatial light modulator (SLM). (b) Scheme of the detection of the Poincaré beams: optical elements are configured as polarizing filters and digital camera (CCD) images the transmitted beam.

The two beams illuminated a Holoeye model SR-2500 spatial light modulator (SLM) at near normal incidence. The SLM was programmed with the spatial-mode patterns used in the production of the Poincaré beam. The figure shows a sample of the patterns used to produce a monstar singularity. Following Eq. 4, the beam that was incident on the right pane of the SLM was simply diffracted at an angle of about 0.5 degrees. The other beam was incident on a pane of the SLM that was programmed with the forked diffraction pattern to generate the proper superposition of $\ell = \pm 1$ beams. The patterns on the left pane were amplitude modulated to produce a purer mode. The diffraction periodicity and phase-blaze of the two patterns encoded on the SLM was the same. The insert to Fig. 4 shows increased periodicity for illustration purposes. We took data with and without amplitude modulation of patterns. β and γ were encoded into the patterns, as specified by Eq. 4.

A half-wave plate rotated the polarization of the pure Gaussian beam diffracted by the SLM. Given the losses due to unwanted reflections and diffraction, the half-wave plate also served to adjust the relative intensities of the two beams. The beams were combined with a mirror and polarizing beam splitter, with the latter serving as the output port of the interferometer and allowing only the horizontally polarized component of the Gaussian beam to proceed through the proper port. A quarter-wave plate, with axis at 45 degrees to the horizontal, placed after the output port of the interferometer put each beam in a circularly polarized state, and thus constructing the mode of Eq. 4.

The resulting beam was imaged with a digital camera. The state of polarization of each point was extracted from a set of six images taken each with a polarization filter (horizontal, vertical, diagonal, antidiagonal, right circular, and left circular), as shown in Fig. 4b. These images were processed to obtain the Stokes parameters of each image point.

4. Results and Discussion

Figure 5 shows a summary of the results. We present both the theoretical simulations and the actual measurements for different values of β (with $\gamma = \pi$ and $\delta = 0$). The images of the intensities of the Poincaré beams have superimposed drawings of the computed polarization states of the light at periodic intervals. We also include dashed-line guides denoting the predicted separatrices for all cases. The ellipse drawings were obtained from the Stokes parameters.

A first glance at the comparison between predicted and measured intensities shows a greater intensity contrast in the data as compared to the prediction. However, we verified that the intensities of the simulations matched the data by comparing the radius at which the polarization was linear. The discrepancy may be due to the lack of purity in the spatial mode; often the diffracted modes are in a superposition of Laguerre-Gauss modes of same axial constant ℓ but distinct radial constant p , which could well be the case here. However, this does not affect the comparison of the polarization-state orientations, which is the main point of interest.

Frames for $\beta = 0$ and $\beta = 90^\circ$ correspond to lemon and star patterns; those for $\beta = 25^\circ$ and $\beta = 30^\circ$ are monstars, and the frame with $\beta = 45^\circ$ is the only mode without a C-point. One can see that the ellipses' orientations in the measured frames indeed rotate as expected in the simulations. We also see qualitative agreement between the predicted and the measured patterns; and the production of monstars for $\beta = 25^\circ$ and $\beta = 30^\circ$ is unquestionable.

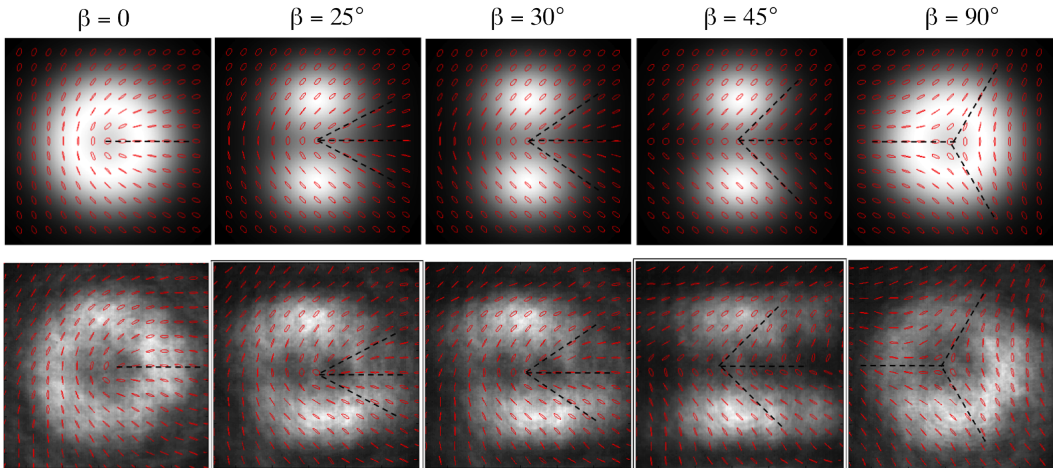


Fig. 5. Comparison between simulations (first row) and measurements (second row) for different values of β . Ellipses are computed state of polarization at the location. Dashed lines are the separatrices corresponding to each case (numerical values given in Table 2).

A closer analysis of the ellipse orientations, in particular as it respects the comparison of the patterns around the predicted separatrices, given in Table 2, shows remarkable agreement between the simulations and the experimental results. The frame for $\beta = 45^\circ$ corresponds to an interesting case. It is a case that is the transition between monstars and stars, a case where the ellipses orientation switches from rotating in one sense to rotating in the other sense, discontinuously. The case is itself singular: it does not contain a C-point because there is no optical vortex in the spatial mode.

In summary, we have shown a method to produce C-point singularities of any kind on demand, centered on an optical beam. We also demonstrated the production of monstars, which have been elusive to laboratory implementations with tailored beams. Comparisons between experimental results and expectations are very good. The results suggest interesting work ahead, involving higher-order spatial modes, producing C-points with high index I_C . The latter may be difficult due to the extreme sensitivity of optical vortices to break up into individual singly-charged vortices. Propagation effects include the transformation of the C-points as the beams propagate due to Gouy phase. Besides their intrinsic interest, polarization singularities could become a means of making sensitive measurements, since their dark components, optical vortices, are very sensitive to perturbations [3, 20].

Table 2. Angles (in degrees) subtended by C-point separatrices ϕ_i with $\delta = 0$.

β	γ	ϕ_1	ϕ_2	ϕ_3
0	180	0		
18.43	180	0	0	0
25	180	0	+27.5	-27.5
30	180	0	+34.3	-34.3
44.9	180	0	+45	-45
90	180	180	+60	-60
55	180	180	+49.3	-49.3
20	270	-15		
60	270	216.7	78.5	-25.2

We acknowledge support from the National Science Foundation, , Research Corporation, and U.S. Air Force contract FA8750-11-2-0034. We thank M. Dennis, G. Milione and N. Viswanathan for help and stimulating discussions.

References

1. J.F. Nye, *Natural Focusing and Fine Structure of Light* (IOP, 1999).
2. M.V. Berry and J.H. Hannay, "Umbilic points on Gaussian random surfaces," *J. Phys. A* **10**, 1809–1821 (1977).
3. E.J. Galvez, B.L. Rojec, and K.R. McCullough, Imaging optical singularities: Understanding the duality of C-points and optical vortices, *Proc. SPIE* **8637**, 863706 (2013).
4. E.J. Galvez, B.L. Rojec, V. Kumar, and N. Viswanathan (to be published).
5. M.S. Soskin, V. Denisenko, and I. Freund, "Optical polarization singularities and elliptic stationary points," *Opt. Lett.* **28**, 1473–1477 (2003).
6. F. Flossmann, U.T. Schwarz, M. Maier, and M.R. Dennis, "Polarization Singularities from Unfolding an Optical Vortex through a Birefringent Crystal," *Phys. Rev. Lett.* **95**, 253901 1-4 (2005).
7. R.I. Egorov, M.S. Soskin, D.A. Kessler, and I. Freund, "Experimental Measurements of Topological Singularity Screening in Random Paraxial Scalar and Vector Optical Fields," *Phys. Rev. Lett.* **100**, 103901 1–4 (2008).
8. F. Flossmann, K. O'Holleran, M.R. Dennis, and M.J. Padgett, "Polarization Singularities in 2D and 3D Speckle Fields," *Phys. Rev. Lett.* **100**, 203902 1–4 (2008).
9. A.M. Beckley, T.G. Brown, and M.A. Alonso, "Full Poincaré beams," *Opt. Express* **18**, 10777–10785 (2010).
10. F. Cardano, E. Karimi, S. Slussarenko, L. Marrucci, C. de Lisio, and E. Santamato, "Polarization pattern of vector vortex beams generated by q-plates with different topological charges," *Appl. Opt.* **51**, C1-C6 (2012).
11. E.J. Galvez, S. Khadka, W.H. Schubert, and S. Nomoto, "Poincaré-beam patterns produced by nonseparable superpositions of LaguerreGauss and polarization modes of light," *Appl. Opt.* **51**, 2925-2934 (2012).
12. E.J. Galvez and S. Khadka, "Poincaré modes of light," *Proc. SPIE* **8274**, 82740Y 1-8 (2012).
13. V. Kumar, G.M. Philip and N.K. Viswanathan, Formation and morphological transformation singularities: Hunting the monstar, *J. Opt.* **15**, 044027, (2013).
14. M.R. Dennis, "Polarization singularities in paraxial vector fields: morphology and statistics," *Opt. Commun.* **213**, 201–221 (2002).
15. M.R. Dennis, "Polarization singularity anisotropy: determining monstardom," *Opt. Lett.* **33**, 2572–2574 (2008).
16. M. J. Padgett and J. Courtial "Poincare -sphere equivalent for light beams containing orbital angular momentum," *Opt. Lett.* **24**, 430-432 (1999).
17. S.M. Baumann, D.M. Kalb, L.H. MacMillan, and E.J. Galvez, "Propagation dynamics of optical vortices due to Gouy phase," *Opt. Express* **17**, 9818–9827 (2009).
18. D.M. Kalb and E.J. Galvez, "Composite Vortices of displaced Laguerre-Gauss beams," *Proc. SPIE* **7227**, 72270D 1-8 (2009).
19. E.J. Galvez "Applications of Geometric Phase in Optics" in *Recent Research Developments in Optics*, **2**, 165-182 (2002).
20. F. Ricci, W. Löffler, and M.P. van Exter, "Instability of higher-order optical vortices analyzed with a multipinhole interferometer," *Opt. Express* **20**, 22961–22975 (2012).